AN INVESTIGATION OF SLAM EVENTS IN TWO DIMENSIONS USING SMOOTHED PARTICLE HYDRODYNAMICS

Daniel J. Veen and Tim P. Gourlay

Centre for Marine Science and Technology, Curtin University of Technology, Perth, Western Australia

ABSTRACT

Smoothed Particle Hydrodynamics (SPH) is a mesh-free Lagrangian computational method suited to modelling fluids with a freely deforming surface. In the present work, SPH has been applied to the problem of slamming, focusing particularly on the impact of two dimensional wedge forms on a free surface contained in a hydrostatic tank. Results from the wedge simulations have shown good agreement with previous experimental studies, paving the way for the work to be extended to mono-hull and catamaran hull forms. The completed validation of the SPH algorithm as applied to the two-dimensional dam beak test case is also discussed.

1. INTRODUCTION

Slamming of mono-hull and multi-hull ships can cause significant structural and payload damage due to the loads and subsequent whipping experienced. Occurring predominantly at the bow, slams are due to the relative vertical motion between the hull and the water surface. Few full scale studies of slam events have been published, but one of note conducted by Thomas et al (2003) monitored slam loads on an 86m Incat catamaran ferry on a sector of its delivery voyage, finding the greatest loads experienced by the structure were attributed to wet deck slams as opposed to bow slams.

A study completed by Whelan (2004) looked more closely at the slamming phenomenon. Whelan conducted a series of drop tests on a variety of hull forms ranging from a simple wedge, to those including side panels and finally hull forms similar to those currently in service on a variety of Incat catamarans. The experimental apparatus mounted the model on a ram which could be released from a variety of drop heights into a large tank. This series of drop tests was designed to replicate a cross sectional form impacting the water surface and is therefore a good benchmark for validation purposes.

Modelling events such as the Whelan drop test using computational fluid dynamics (CFD) has met with limited success in grid based methods due to the inability of most codes to accurately represent a freely deforming surface. Smoothed Particle Hydrodynamics (SPH) is a relatively new CFD method capable of modelling free and breaking surfaces. Developed independently by Lucy (1977) and Gingold and Monaghan (1977), SPH was originally applied to the problem of fission in rapidly rotating stars due to its ability to model both large changes in spatial and density scales, and problems without definite boundaries. The absence of a computational grid within SPH lends the method to many other areas of numerical fluid dynamics modelling, including free surface flows and fluid structure interactions.

SPH has only recently been used to model fluid flows due to the computing power required, but has shown great promise when simulating violent impacts including sloshing (Pákozdi 2007) and green-water events (Gomez-Gesteira et al 2005).

2. SPH MODEL DESCRIPTION

2.1 Integral Interpolation in SPH

The SPH method is based on the integral interpolation of a function at fixed points represented by particles, which for any function is given by:

$$A(\mathbf{r}) \approx \int A(\mathbf{r}')W(\mathbf{r}' - \mathbf{r})d\mathbf{r}' \tag{1}$$

This approximation of A at the point of interest $\mathbf{r}$ becomes exact as the kernel W approaches the Dirac delta function. However for SPH applications, a slightly broader kernel function is implemented, encompassing a number of particles in a small region rather than just the single point of interest. The broadness of the kernel is defined through the *smoothing length*, represented by the variable h. Written in the form of a discrete summation over neighbouring particles b with volume $dV_{\mathbf{r}'}$, Eq. (1) becomes:

$$A(\mathbf{r}) = \sum_b A(\mathbf{r}')W(\mathbf{r}' - \mathbf{r}; h)dV_{\mathbf{r}'} \tag{2}$$

The approximation of the delta function has taken many forms in SPH literature, notably piecewise spline and Gaussian functions. Morris et al (1997) found that spline functions carried inherent instabilities which decreased as the order of the spline was increased. However, increasing the order introduces negative kernel values at particular values of $\mathbf{r}' - \mathbf{r}$ so a function of Gaussian form for d dimensions, Eq. (3), is more suited to the interpolation.

$$W(\mathbf{r}' - \mathbf{r}, h) = \left(\frac{1}{h\sqrt{\pi}}\right)^d e^{-\frac{|\mathbf{r}'-\mathbf{r}|}{h^2}} \tag{3}$$

Before inclusion in the SPH model, a modification to the Gaussian kernel is required to improve computational efficiency (Landrini et al 2003). To reduce the total number of particle interactions the kernel is cut off at a radius of 3h and then normalised in two dimensions to give:

$$W(\mathbf{r}' - \mathbf{r}, h) = \frac{e^{-\frac{|\mathbf{r}'-\mathbf{r}|}{h^2}} - e^{-9}}{h^2\pi(1 - 10e^{-9})} \tag{4}$$

2.2 SPH Equations of Motion

For free surface flows, the classical Navier-Stokes equations are solved. However, all of the models presented are assumed inviscid and so the system of equations reduces to the Euler equations for momentum and continuity:

$$\frac{d\mathbf{u}}{dt} = -\frac{1}{\rho}\nabla P + \mathbf{g} \tag{5}$$

$$\frac{d\rho}{dt} = -\rho\nabla \cdot \mathbf{u} \tag{6}$$

where ρ is the fluid density, P the pressure, $\mathbf{u}$ the fluid velocity and $\mathbf{g}$ the acceleration due to gravity. Applying the interpolation to the Euler equations gives the SPH momentum and continuity equations for particle a summed over N neighbours of mass m_b:

$$\frac{d\mathbf{u}_a}{dt} = -\sum_{b=1}^{N} m_b \left(\frac{P_a}{\rho_a^2} + \frac{P_b}{\rho_b^2}\right) \boldsymbol{\nabla}_a W_{ab} \tag{7}$$

$$\frac{d\rho_a}{dt} = -\sum_{b=1}^{N} m_b (\mathbf{u_a} - \mathbf{u_b}) \cdot \boldsymbol{\nabla}_a W_{ab} \tag{8}$$

W_{ab} represents the value of the kernel at particle a due to the neighbouring particle b.

2.3 Equation of State

The SPH method assumes that the fluid is fully compressible, however detailed compressible flow calculations are often not required for nearly incompressible fluids such as water. Most problems involving water are of low flow speed when compared to the speed of sound. This demands a very small time step by the Courant–Friedrichs–Lewy condition, which is not viable in terms of the required computation time. Therefore, for many SPH problems the real fluid is approximated by an artificially compressible fluid through a modified state equation. Eq. (9) is the standard equation of state used in most single phase SPH algorithms, where P_a is the pressure above atmospheric of fluid particle a (Monaghan, 2005).

$$P_a = B\left(\left(\frac{\rho_a}{\rho_0}\right)^{\gamma} - 1\right) \tag{9}$$

To avoid compression effects, the values of γ and the factor B are chosen so that the fluctuations in density are no more than 1% of the reference value ρ_0. This is achieved by setting γ equal to 7 (the approximate value in the seawater equation of state) and setting the sound speed such that the maximum fluid velocity is no greater than Mach 0.1. The factor B (typically 3.04×10^8 Pa for sea water) is directly related to the sound speed, and so in order to reduce the computation time B is then defined using the modified sound speed through Eq. (10).

$$B = \frac{c_s^2 \rho_0}{\gamma} \tag{10}$$

It should be noted that the lower sound speed is capable of creating pressure waves of higher amplitude than those observed experimentally, and can be difficult to eliminate without increasing computation time considerably.

2.4 Numerical Instability

To reduce the level of instability associated with the explicit time integration, an artificial viscous term is included in the momentum equation (Monaghan, 2005). The expression introduces a small shear and bulk viscosity in order to simulate shock problems, but for small values of α and β, Eq. (12), the artificial viscosity Π_{ab} simply stabilises the algorithm.

$$\frac{du_a}{dt} = -\sum_{b=1}^{N} m_b \left(\frac{P_a}{\rho_a^2} + \frac{P_b}{\rho_b^2} + \Pi_{ab} \right) \nabla_a W_{ab} \tag{11}$$

Where Π_{ab} is given by:

$$\Pi_{ab} = \begin{cases} \dfrac{-\alpha \bar{c}_{ab} \mu_{ab} + \beta \mu_{ab}^2}{\bar{\rho}_{ab}}, & \mathbf{u}_{ab} \cdot \mathbf{r}_{ab} < 0 \\ 0, & \mathbf{u}_{ab} \cdot \mathbf{r}_{ab} > 0 \end{cases} \tag{12}$$

$$\mu_{ab} = \frac{h \mathbf{u}_{ab} \cdot \mathbf{r}_{ab}}{\mathbf{r}_{ab}^2 + \varepsilon h^2} \tag{13}$$

The double subscripts ab in Eq. (11) and Eq. (12) represent the interaction between the particle of interest a and a neighbour b (i.e. relative velocity $\mathbf{u}_{ab}$ and average density $\bar{\rho}_{ab}$).

Typical values for α and β in problems not involving shocks are 0.01-0.10 and 0 respectively, but can be as high as 1.0 or 2.0 for complex shock simulations (Monaghan, 2005). Colagrossi and Landrini (2003) compared values of α in a range from 0.005 to 0.1 using a two-dimensional dam break and found 0.03 to be the most appropriate value, maintaining stability without introducing a considerable bulk fluid viscosity. The value of ε in Eq. (13) is small, typically 0.01, and is placed here to avoid a singularity in the unlikely event of the particle separation $\mathbf{r}_{ab}$ approaching zero.

2.5 Density Reinitialisation

Further corrections to the numerical algorithm are necessary in order to counter inconsistencies in the density of the system. The SPH interpolation requires the support volume to be full of particles so as to accurately reproduce the density field. Near free surfaces the kernel does not fill entirely with particles causing a reduction in the local fluid density and a gradual corruption of the entire pressure and density fields.

Belytschko et al (1998) proposed a Moving Least Squares correction to the density field Eq. (14). This reinitialisation of the density is applied approximately every 20 time steps following Colagrossi and Landrini (2003), restoring consistency between particle mass, density and volume.

$$\rho_a = \sum_{b=1}^{N} m_b W^{MLS}(\mathbf{r}_a - \mathbf{r}_b, h) \tag{14}$$

Colagrossi and Landrini (2003) compared the density reinitialisation method against a lower-order Shepard interpolation and found the former to be superior in terms of energy conservation. Re-distributing or re-meshing particles over a grid has been applied by Chaniotris et al (2002) to problems without a freely deformable surface. Defining the free surface position and then re-meshing is computationally intensive and as such this method has not been implemented in the current model.

2.6 Boundary Conditions

Two main types of rigid wall boundary methods are used widely in SPH algorithms. The simpler, and less computationally intensive of the two methods, is to use boundary particles placed evenly along the surface of each wall. Monaghan (2005) uses these particles to exert repulsive forces similar to those found in molecular dynamics, such as the Lennard-Jones force. Although this method is flexible, it does allow some inconsistencies to develop, particularly in the pressure field.

On the other hand, the 'ghost' particle method mirrors fluid particles about the boundary, filling the kernel. The reflected particles are given identical densities, pressures and velocities (parallel to the wall) to that of their corresponding fluid particles. To invoke a pressure gradient to hold fluid particles on one side of the wall, the ghost particles are given the opposite velocity component normal to the wall. This method carries with it a free slip condition and is useful for simple geometries, but becomes more intricate as the geometry complexity increases. Given the relatively simple geometry, ghost particles were used for all boundaries included in the present work.

3. MODEL VALIDATION

The validation process has applied the developed SPH code to a number of inviscid test cases, but only two directly related to fluid impacts are presented. The first case is that of a simple tank holding a volume of fluid (of depth H) steady over an extended period. This problem was designed to give an indication of the stability of the system through analysis of the pressure at varying depths and was of high importance as the drop tests in section 4 were conducted in a similar sized tank. It was found that over a period of $12\sqrt{H/g}$ the pressure throughout the tank oscillated about that expected due to hydrostatic pressure. The amplitude of the pressure oscillations was approximately 0.1% to 0.5% of the original pressure and was due to the boundary condition invoking vibrations, associated with the normal modes of the system, through the tank. This test case proved the ability of the unsteady SPH algorithm to maintain a steady solution over a period of time well in excess of that required to simulate the impacts of the forms discussed in section 4.

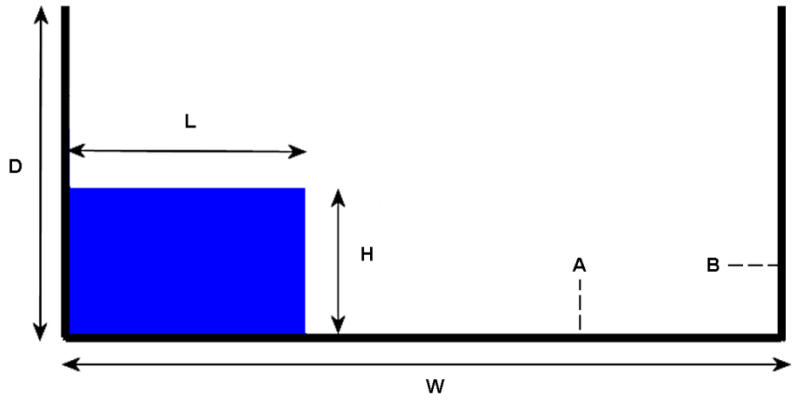

Fig. 1. Schematic diagram of the Dam Break.

Extending the tank model by allowing the right hand retaining wall to be removed at some time *t*, results in the formation of a bore known as the classical dam break (see Fig. 1). An experimental study conducted by Zhou, Buchner and Kat (1999) was used as a basis for the validation process. The experimental dam break was initially set with the reservoir of width $L = 2H$ held behind a movable flap. Upon release, the bore was allowed to travel a distance $3.36H$ along the flume before striking a vertical wall. Zhou et al (1999) placed a series of height and pressure sensors along both the tank floor and the far wall in order to analyse the profile of the advancing bore and the loads experienced by each of the walls.

The SPH simulation of the dam break was designed to emulate the experiment conducted by Zhou et al (1999). The fluid particles were initially arranged on a Cartesian lattice with a depth of $H = 1.0$ m, without the presence of the reservoir wall (it was assumed that at $t = 0$ s the wall was removed). Beginning the simulation without this retaining wall required a correction to the hydrostatic pressure field in order to ensure that the free surface along the right side of the reservoir maintained the same pressure as that of the surrounding fluid. As the dam break was modelled in a void, the pressure at the free surface was set to zero.

Fig. 2 describes the formation and impact of the bore at two moments in time during the $12\sqrt{H/g}$ long simulation. Fig. 2a confirms that the bore maintains a hydrostatic pressure distribution before impact with the far wall. This smooth pressure gradient is a demonstration of the lack of noise associated with the ghost particle boundary method. Previous dam break simulations utilising repulsive force boundary conditions were heavily corrupted by noise in the pressure field, particularly at low resolution. The fluid pressure during run-up is illustrated in Fig. 2b and is shown to be a maximum near the tank corner.

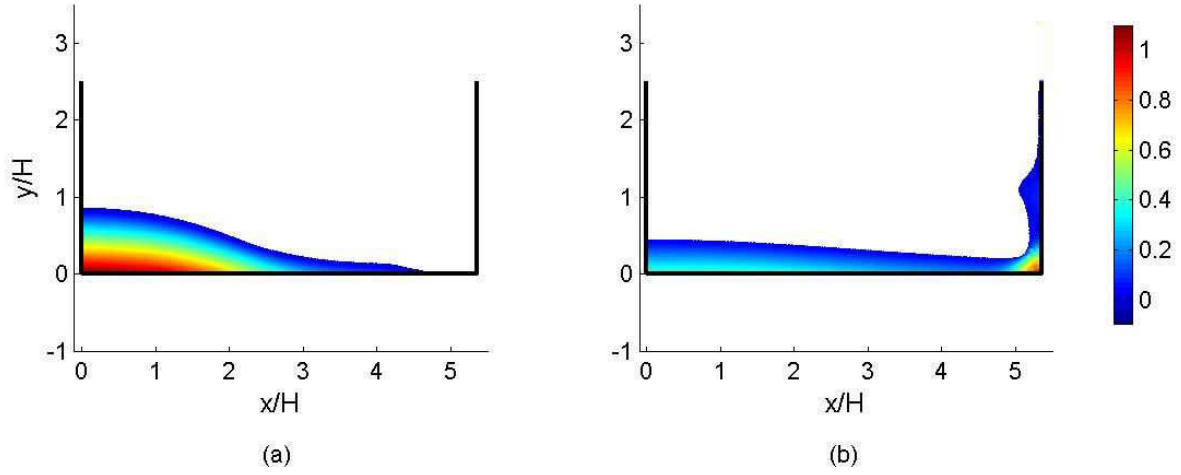

Fig. 2. Formation and Impact of the Dam Break at $t(g/H)^{0.5} = 3.0$ (a) and $t(g/H)^{0.5} = 5.0$ (b) for 45 000 particles at a resolution of 150 particles per unit length. The images are coloured by dimensionless pressure $P/(\rho g H)$

Of the numerous sensors monitoring the dam break in the Zhou et al (1999) experiment, two at significant locations were selected for comparison. Point B (see Fig. 1) 0.16 m above the tank floor was chosen as a suitable location to sample the pressure on the wall near the point of impact. The SPH modelled pressure at B was found to be in reasonable agreement (see Fig. 3a) with the pressure measured at the 0.09 m diameter gauge by Zhou et al (1999). Even so, Zhou et al (1999) reported difficulties in repeatability and so conclusions on the reliability of the SPH model cannot yet be drawn. It should be noted that the large unrealistic

spike in pressure observed at $8\sqrt{H/g}$ is due to the single phase model lacking air to cushion the collapse of the breaking wave after the initial impact (Colagrossi, 2004).

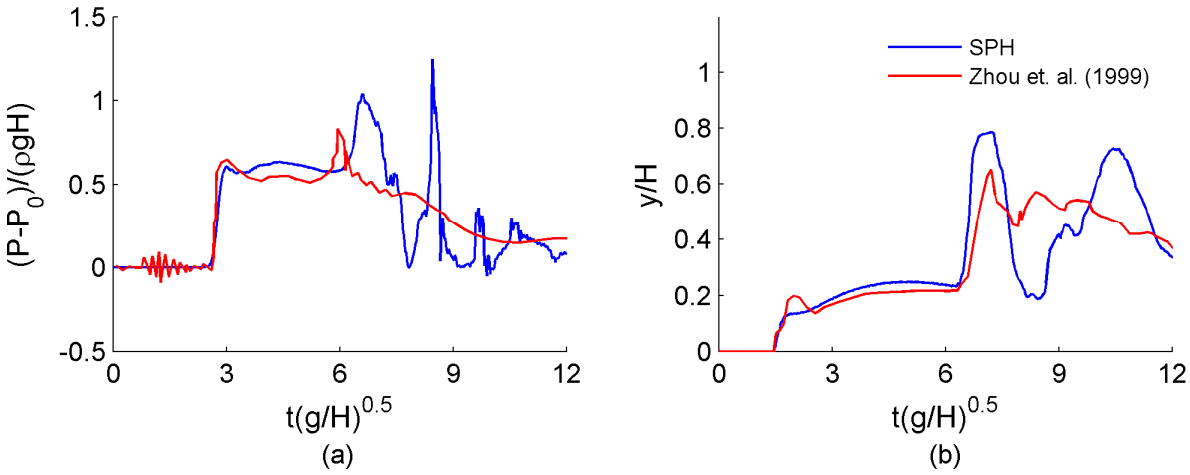

Fig. 3. – The dimensionless pressure on the right tank wall at point B (a) and the height of the bore above position A on the tank floor (b) compared against the experiments of Zhou et al (1999) .

A study of the height of the breaking dam above point A (see Fig. 1) gave further evidence of agreement between the experimental data and SPH model. Point A was located $1.71H$ downstream from the removable reservoir wall and the water level above this point in time is illustrated in Fig. 3b. A sharp initial increase in the height of the toe, followed by a more gradual increase in water depth was observed in both the model and the experiment supporting the validity of the SPH model. Once more Fig. 3b shows that while the SPH model agreed with the experimental water level until approximately $8\sqrt{H/g}$, the collapse of the breaking wave in the single phase model became unrealistic suggesting a coupled air-water model would be more suited to modelling the dam break after the formation of the breaking wave.

4. CURRENT PROGRESS

Prior to beginning SPH simulations with the validated algorithm on multiple hull forms, simple triangular wedge cross sections and their impact with stable free surface were modelled. Whelan (2004) included simple wedge models in the experimental drop tests before extending them to include side plates, a very simple geometry similar to that of a catamaran hull, and ultimately to more recognisable catamaran hull forms. The drop tests were conducted in a tank 2.4 m in length, 1.0 m deep and 0.3 m wide. The widths of the models tested were all fractionally smaller than the tank width (in the order of 1.0 mm) with the purpose of reducing venting from the sides, giving rise to approximately two-dimensional results.

Each of the drop tests were released from a normalised height H^* of 0.89 by Eq. (15) (where l is the beam and h the drop height), which equates to a distance of 0.2 m above the water surface. Due to the presence of friction in the experiment, the model hull forms were unable to fall freely resulting in lower than expected impact speeds. This can clearly be seen in Fig. 4 where the experimental acceleration is less negative than that of the numerical SPH model for the first 0.02 s. Subsequently, the wedge models in the SPH simulation were dropped from a much lower height to ensure the impact velocities of model and experiment were comparable.

$$H^* = \sqrt{\frac{2h}{l}} \tag{15}$$

$$m^* = \frac{m}{\rho w l^2} \tag{16}$$

Calculations of the acceleration of the body require its mass to be known. Whelan (2004) provides a normalised mass m^* of 0.29 for each of the models studied in the present work, which is a function of the model mass m, the fluid density ρ, the width of the model w and the beam l. By Eq. (16), the models simulated using SPH were assumed to have a mass of 74.0 kg/m.

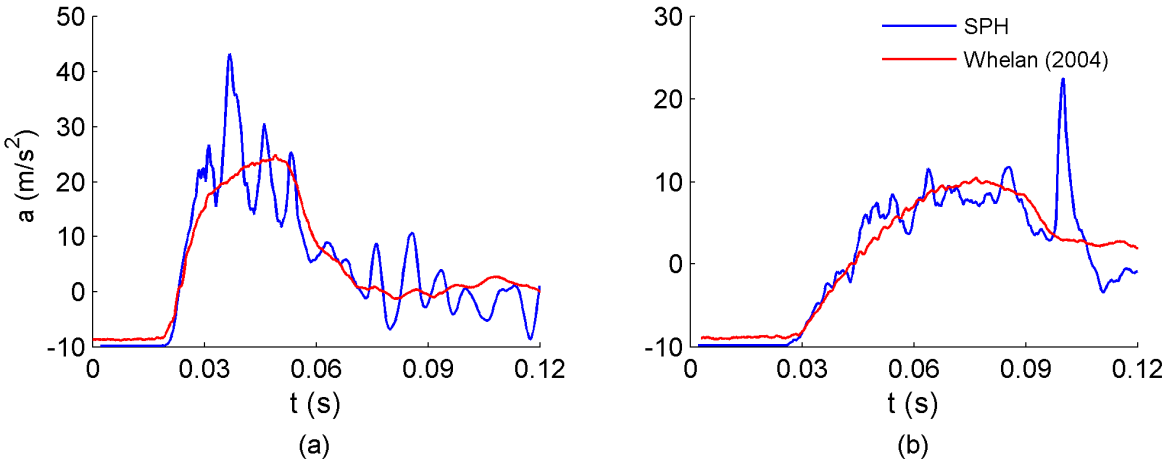

Fig. 4. Acceleration of the body as a function of time for the 15 degree (a) and 25 degree (b) wedges compared with experimental studies by Whelan (2004).

.

The acceleration of two wedges, subtending angles of 15^o and 25^o from the horizontal are depicted in Fig. 4. The SPH results were obtained using a tank of the same dimensions as Whelan (2004) filled with 150 000 particles at a resolution of 250 particles per unit length (viscous effects were ignored due to the short duration of the impact). As the models were just 0.5 m wide, the number of particles close to the surface of the object was comparable with previous studies involving impacts such as the dam break. The compressible nature of the SPH algorithm does cause large amplitude pressure waves to propagate away from the wedge (see Fig. 5) which in turn produce significant oscillations in the acceleration. However, despite the large amplitude oscillations, the acceleration traces in Fig. 4 (particularly that of the 25^o wedge) agree well with the experimental results of Whelan (2004).

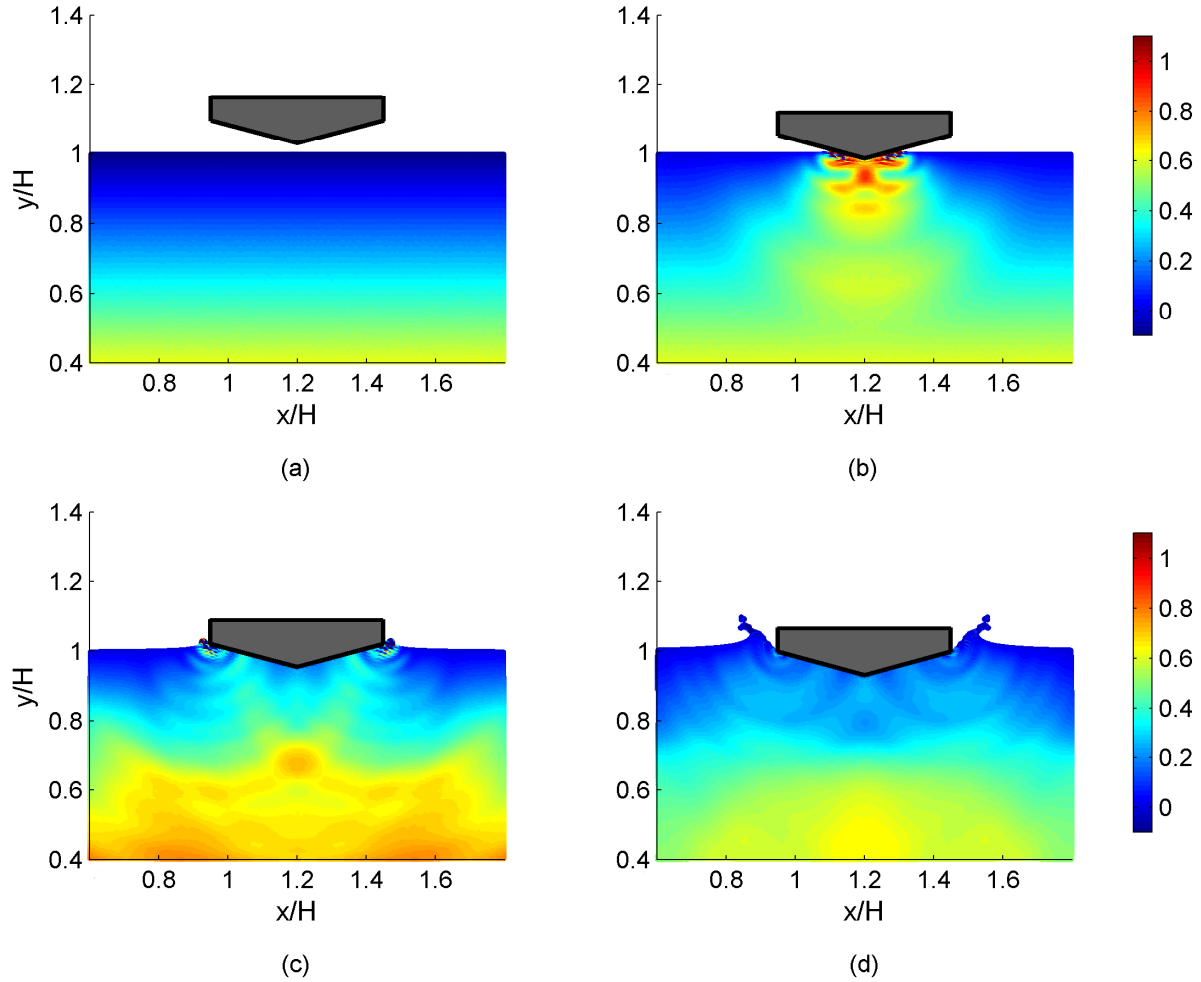

Fig. 5. Four images in time of the impact of a 15 degree wedge impact at (a) t = 0.0s, (b) t = 0.03s, (c) t = 0.06s and (d) t = 0.09s. The images are coloured by dimensionless pressure $P/(\rho g H)$.

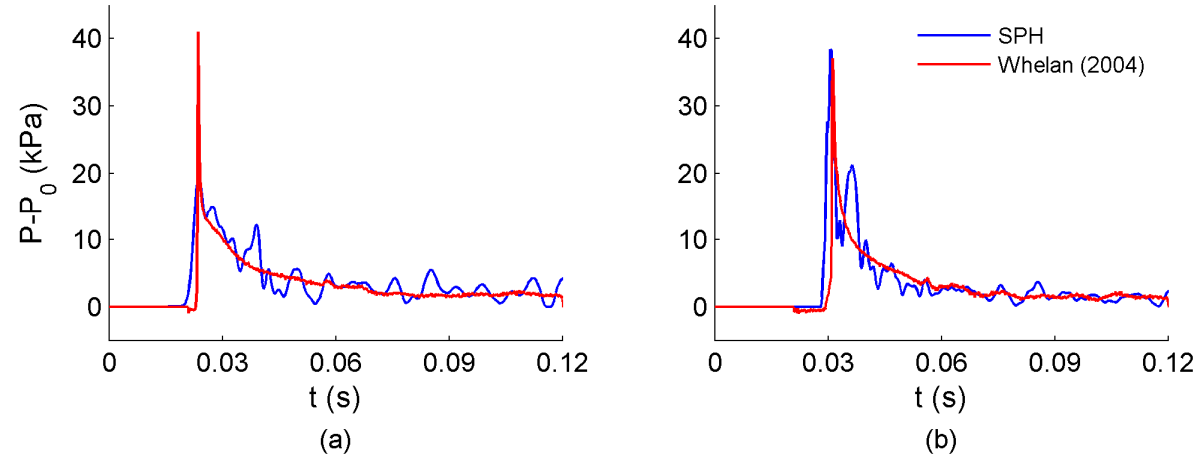

Fig. 6. Pressure at points (a) P_1, 0.02m from the lower vertex, and (b) P_2, 0.10m from the lower vertex on the 15 degree wedge surface.

Pressure transducers were placed at three locations along the 15^o wedge by Whelan (2004). Numerical sensors were then placed at identical positions along the surface of the SPH wedges and the results compared with the experimental pressures in Fig. 6. At point P_2, located 0.10 m from the lower vertex, the peak pressures occurred within 0.002s and were comparable at approximately 38 kPa. The general trend of the pressure at both sensors followed that of the experimental data, with some oscillations due to the aforementioned pressure waves. Increases in particle resolution (by reducing the particle size) of the model have reduced the amplitude of these oscillations, but it is unlikely that without computationally inefficient increases in sound speed that the fluctuations will reduce to experimental size amplitudes using a compressible SPH algorithm.

5. CONCLUSIONS

The Lagrangian SPH algorithm has been validated against a number of test cases, including that of a breaking dam. Studies of the profile of the propagating bore and the impact pressures recorded at the far wall were shown to be in agreement with experiments conducted by Zhou et al (1999). SPH was then used model the problem of slamming through the impact of a two dimensional wedge upon a free surface. Preliminary comparisons with the results of Whelan (2004) have shown good agreement in terms of the acceleration of the body after impact and the pressures experienced at a number of points along the surface of the wedge.

6. FUTURE WORK

The current SPH model will be extended to allow larger numbers of particles to be modelled and the experimental drop tests of various hull shapes examined by Whelan (2004) will be replicated. Examples of two of the proposed hull shapes are given in Fig. 7, including a 25^o wedge with side plates (top) and a symmetric hull with a rounded voluminous centre bow (bottom). Air will then be introduced in order to create a coupled algorithm to simulate venting and entrainment in the arches and corners of the test models.

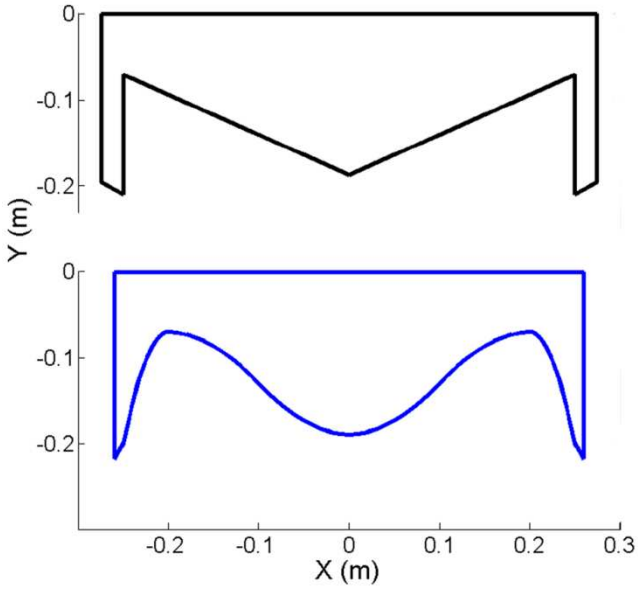

Fig. 7. Sample catamaran hull forms.

Multiple two dimensional equi-spaced models will then be combined to calculate the loads on the forward part of a variety of hull forms in a method similar to strip theory. Ultimately, the model will be extended to three dimensions and applied to the aforementioned validation cases and finally to the experimental tests conducted by Whelan (2004). The result will be a SPH algorithm that can be applied to a variety of hull shapes in both two and three dimensions.

ACKNOWLEDGEMENTS

The authors would like to thank Dr James Whelan (INTEC Engineering, Australia) for providing the drop test data and for his well-heeded advice, and Dr Csaba Pákozdi (Marintek, Norway) for sharing his wealth of knowledge on all things SPH.

References

Belytschko, T.K., Krongauz, Y., Dolbow, J., Gerlach, C., (1998). 'On the Completeness of Meshfree Particle Methods.' International Journal on Numerical Methods in Engineering. **43**: 785-819.

Chaniotris, A. K., (2002). 'Remeshed Smoothed Particle Hydrodynamics for the Simulation of Viscous and Heat Conducting Flows.' Journal of Computational Physics **182**: 67-90.

Colagrossi, A. (2004). 'A Meshless Lagrangian Method for Free-Surface and Interface Flows with Fragmentation.' Rome, Universita di Roma. Doctoral Thesis.

Colagrossi, A., Landrini, M., (2003). 'Numerical Simulation of Interfacial Flows by Smoothed Particle Hydrodynamics.' Journal of Computational Physics **191**: 448-475.

Gingold, R.A., Monaghan J.J., (1977). 'Smoothed Particle Hydrodynamics: Theory and Application to Non Spherical Stars.' Monthly Notices of the Royal Astronomical Society **181**: 375-389.

Gomez-Gesteira, M., Cerqueiro, D., Crespo, A.J.C., Dalrymple, R.A., (2005). 'Green Water Overtopping Analysed with a SPH Model.' International Journal of Ocean Engineering **32**: 223-238.

Landrini, M., Colagrossi, A., Faltinsen, O., (2003). Sloshing in 2-D Flows by the SPH Method. The 8th International Conference on Numerical Ship Hydrodynamics. Busan, Korea.

Lucy, L., (1977). 'A Numerical Approach to Testing the Fission Hypothesis.' Astronomical Journal **82**: 1013-1024.

Monaghan, J.J., (2005). 'Smoothed Particle Hydrodynamics.' Reports on Progress in Physics **68**: 1703-1759.

Morris, J. P., Fox, P. J., Zhu, Y., (1997). 'Modelling Low Reynolds Number Incompressible Flows Using SPH.' Journal of Computational Physics **136**: 214-226.

Pákozdi, C., (2008). 'A Smoothed Particle Hydrodynamics Study of Two-Dimensional Nonlinear Sloshing in Rectangular Tanks'. Department of Marine Technology. Trondheim, Norwegian University of Science and Technology. Doctoral Thesis.

Thomas, G. A., Davis, M. R., Holloway, D.S., Watson, N.L., Roberts, T.J., (2003). 'Slamming Response of a Large High-Speed Wave-Piercer Catamaran.' Marine Technology **40**(2): 126-140.

Whelan, J. R. (2004). 'Wetdeck Slamming of High-Speed Catamarans with a Centre Bow'. School of Engineering, University of Tasmania. Doctoral Thesis.

Zhou, Z. Q., De Kat, J. O., Buchner, B., (1999). 'A Nonlinear 3-d Approach to Simulate Green Water Dynamics on Deck'. Proceedings of the 7th International Conference on Numerical Ship Nantes, France.